iScience

CellPress
OPEN ACCESS

Article

Developmental regulation of oocyte lipid intake through 'patent' follicular epithelium in *Drosophila melanogaster*

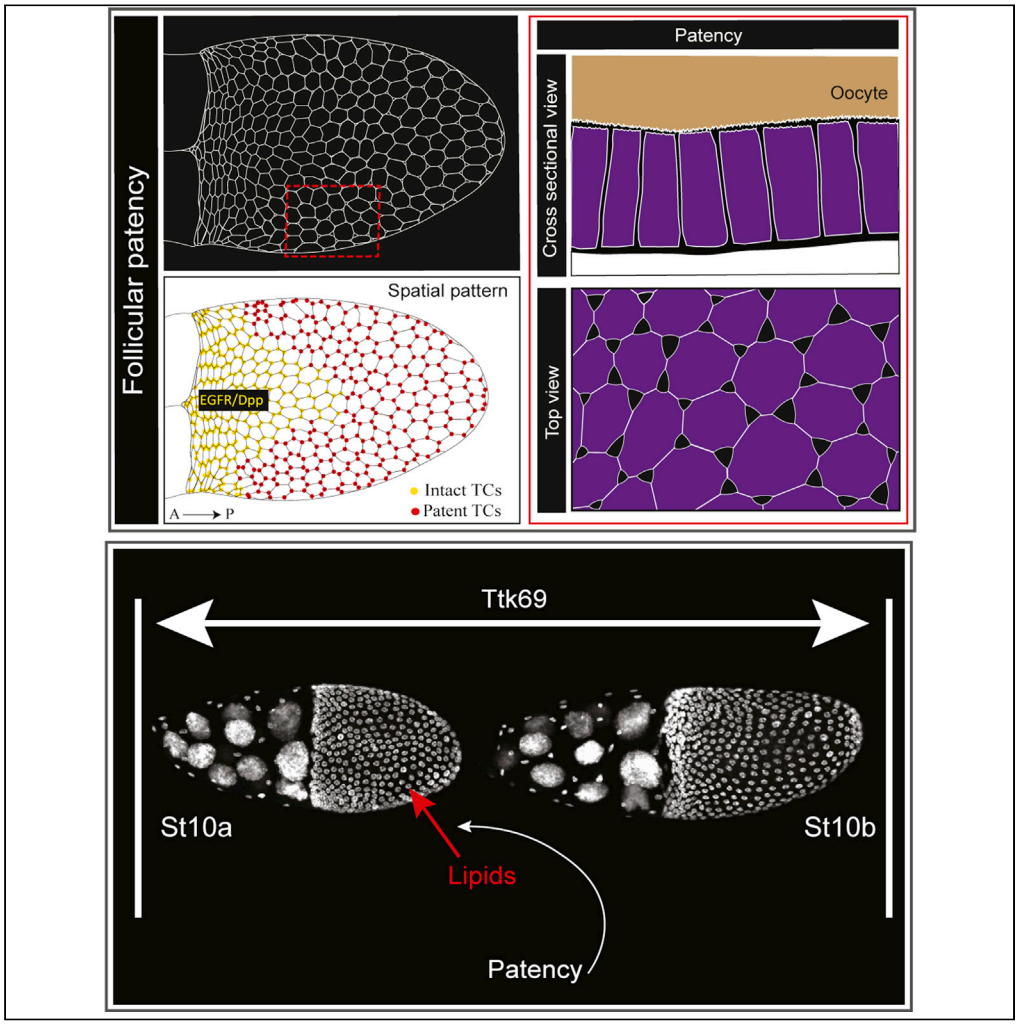

Sarayu Row, Yi-Chun Huang, Wu-Min Deng

wdeng7@tulane.edu

Highlights

Drosophila FE exhibits patency, creating transient channels across the monolayer

Patency aids in transepithelial transport of lipids for normal oocyte growth

Ttk69 regulates the temporal range of patency

EGFR and Dpp patterning pathways influence the specific spatial pattern of patency

Row et al., iScience *24*, 102275
April 23, 2021
https://doi.org/10.1016/j.isci.2021.102275

iScience

CellPress
OPEN ACCESS

Article

Developmental regulation of oocyte lipid intake through 'patent' follicular epithelium in *Drosophila melanogaster*

Sarayu Row,[1] Yi-Chun Huang,[2] and Wu-Min Deng[1,2,3,*]

SUMMARY

Epithelia form protective permeability barriers that selectively allow the exchange of material while maintaining tissue integrity under extreme mechanical, chemical, and bacterial loads. Here, we report in the *Drosophila* follicular epithelium a developmentally regulated and evolutionarily conserved process "patency", wherein a breach is created in the epithelium at tricellular contacts during mid-vitellogenesis. In *Drosophila*, patency exhibits a strict temporal range potentially delimited by the transcription factor Tramtrack69 and a spatial pattern influenced by the dorsal-anterior signals of the follicular epithelium. Crucial for growth and lipid uptake by the oocyte, patency is also exploited by endosymbionts such as *Spiroplasma pulsonii*. Our findings reveal an evolutionarily conserved and developmentally regulated non-typical epithelial function in a classic model system.

INTRODUCTION

Epithelial integrity is maintained through a range of processes such as cell division, apoptosis, and morphogenetic movements (Guillot and Lecuit, 2013; Tai et al., 2019), and the preservation of tricellular contacts (TCs) between the epithelial cells in a tissue is key to maintaining its physical and electrochemical barrier function (Bosveld et al., 2008). The epithelium is also permeable, allowing selective passage of material via transcellular and paracellular routes (Powell, 1981). Failure to maintain TCs has been reported to promote metastasis of cancer cells by causing cells to delaminate from epithelial tumors (Dunn et al., 2018; Jang et al., 2007). Loss of TCs is also associated with Crohn disease (Maloy and Powrie, 2011). The extensively characterized *Drosophila* follicular epithelium (FE) surrounding developing egg chambers provides an excellent *in vivo* model to study TCs and their role in balancing barrier function and permeability in epithelial monolayers.

As the developmental unit of oogenesis, each egg chamber in the *Drosophila* ovary comprises an oocyte and 15 nurse cells, all enclosed in the FE monolayer, and the presence of nurse cells distinguishes the ovaries in *Drosophila* as "meroistic" (King and Koch, 1963; Klowden, 2013). A string of sequentially developing egg chambers is contained in each of the 16 ovarioles in each ovary, beginning with the germarium and advancing from stages 1 through 14 (King and Koch, 1963) (Figure 7). The FE monolayer protects and supports germline development while undergoing a series of spatiotemporally regulated morphogenetic movements to pattern and form egg chambers and secretes the chorion, an eggshell component (Dobens and Raftery, 2000; King and Koch, 1963). Vitellogenic stages (stage (St) 8–12) are characterized by the trans-epithelial movement of hemolymph-borne yolk proteins (YPs) into the oocyte. YPs are synthesized primarily in the fat body, are secreted into the hemolymph, travel between the follicle cells to reach the oocyte membrane, and are internalized via receptor-mediated endocytosis (Bownes et al., 1993; DiMario and Mahowald, 1987; Richard et al., 2001). The FE also synthesizes YPs in small amounts until St 11 when it switches to chorion secretion (Isaac and Bownes, 1982; Weiner et al., 1982). Other materials carried by the hemolymph also enter the oocyte, such as lipophorins and endosymbionts (Herren et al., 2013; Tufail and Takeda, 2009), but the mechanistic details of this trans-epithelial FE transport in *Drosophila* remain unclear.

In this study, we describe a developmentally regulated process in the FE at mid-oogenesis termed "patency", a phenomenon previously unreported in *Drosophila*. Patency is defined as the opening of intercellular spaces between follicle cells that allows the penetration of hemolymph proteins into the oocyte

[1]Department of Biological Science, Florida State University, Tallahassee, FL 32306-4295, USA

[2]Department of Biochemistry and Molecular Biology, Tulane University School of Medicine, New Orleans, LA 70112, USA

[3]Lead contact

*Correspondence: wdeng7@tulane.edu

https://doi.org/10.1016/j.isci.2021.102275

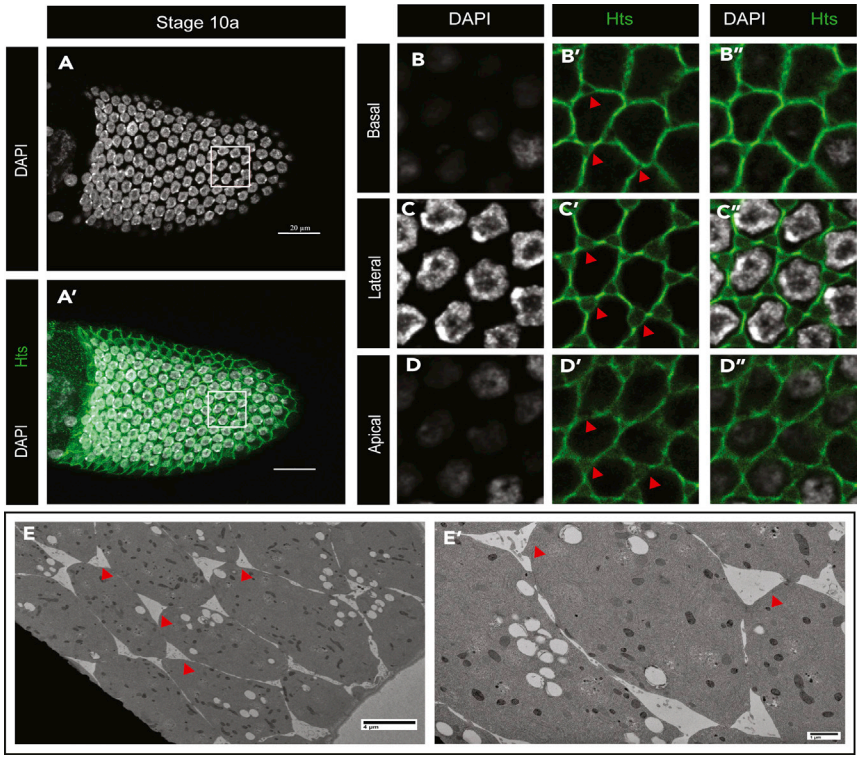

Figure 1. Patency in *Drosophila melanogaster*

(A and A′) Stage 10a oocyte-associated FE. White box is expanded in (B-D″); Scale bars, 20 μm.

(B–B″, C–C″, and D–D″) Basal, lateral, and apical view, respectively, of the TC gaps in the oocyte-associated FE at St 10a. Hts (Hu li tai shao, adducin) marks the membrane; DAPI marks the nuclei.

(E and E′) TEM images of the surface of a St 10a FE. TC gaps indicated by red arrowheads. Scale bars: (E) 4μm, (E′) 1μm.

during the vitellogenic stages of oogenesis (Telfer, 1961; Zimowska et al., 1994). Unlike in other insects, patency in *Drosophila* is only present in mid-vitellogenesis. This reduced temporal range appears to be regulated at least in part by the BTB (Broad-Complex, Tramtrack and Bric a brac) transcription factor Tramtrack69 (Ttk69). We also report a consistent spatial pattern of patency in the FE, influenced by the signaling pathways that pattern the dorsal anterior. Moreover, we found that the spatiotemporal patterns of patency are also present in the sister species, *Drosophila simulans* (*D. simulans*). Together, our results reveal a developmentally regulated function of the FE, wherein openings or channels are transiently created for trans-epithelial material transfer and normal oocyte growth.

RESULTS

Drosophila follicular epithelium exhibits "patency"

While examining wild-type (WT) *Drosophila melanogaster* egg chambers, we noticed an anomalous but consistent feature—the opening of the TCs in mid-vitellogenic FE. These TC "gaps" are observed at the basal, lateral, and apical domains of the FE (Figures 1A–1D″, S1B, and S1D–S1H), spanning the epithelial monolayer and effectively creating a breach in the epithelium. We verified the appearance of TC gaps in the *Drosophila* FE using a detergent-free immunostaining protocol, as well as transmission electron microscopy (TEM) (Figures S1A–S1A‴, 1E, and 1E′). Although not previously described in *Drosophila*, several insect species have been reported to exhibit "patency", a phenomenon characterized by the opening of intercellular contacts between follicle cells for oocyte yolk uptake during vitellogenesis (Pratt and Davey, 1972). Together with our data in the *Drosophila* FE, we therefore concluded that that the *Drosophila* FE also exhibits patency during oogenesis.

Next, to determine whether the TC gaps affect the permeability of the FE, we imaged live egg chambers incubated with FITC (Fluorescein isothiocyanate) labeled dextran to visualize the gaps in real time. The

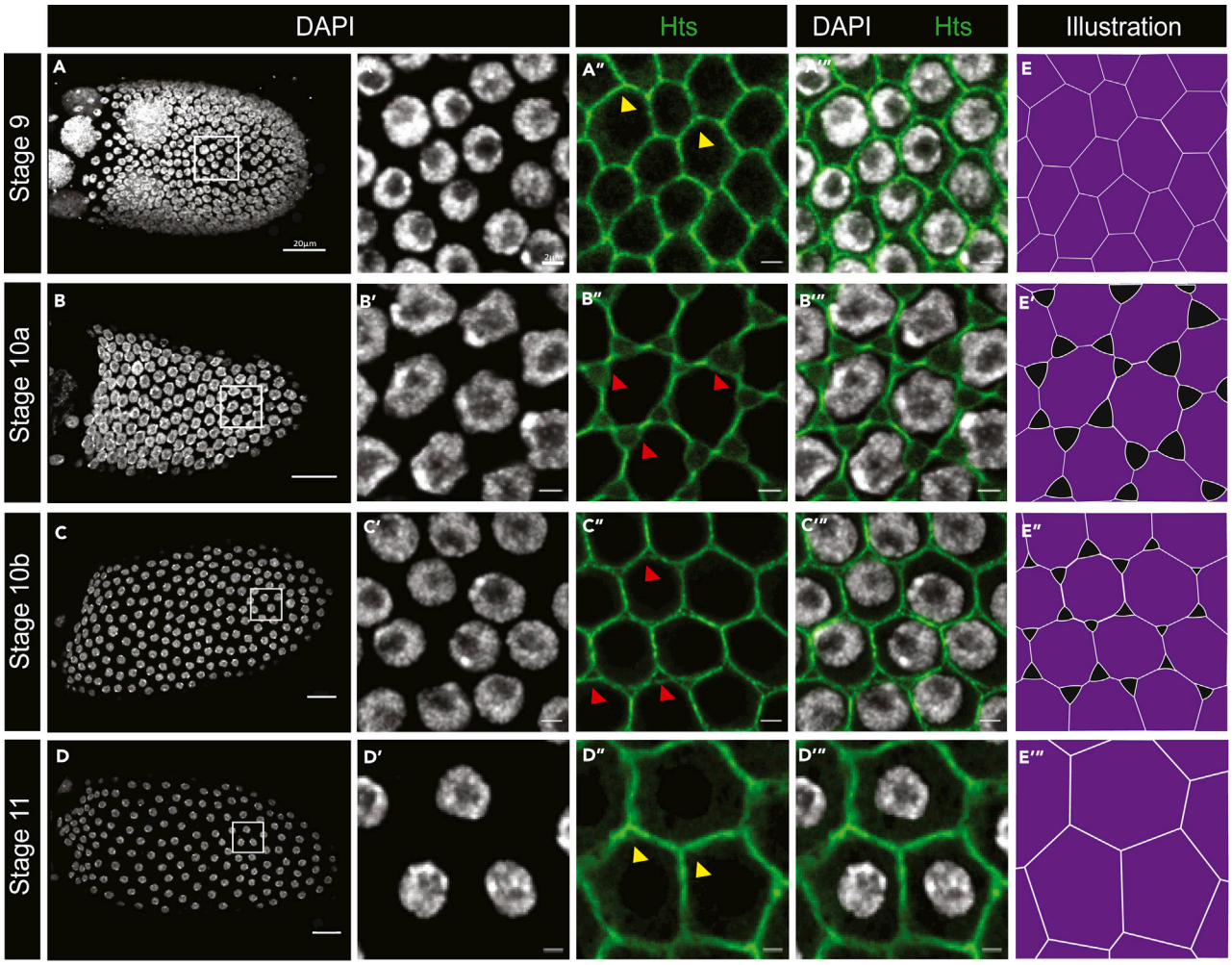
DAPI
Hts
DAPI Hts
Illustration
Stage 9
Stage 10a
Stage 10b
Stage 11
A
A′
A″
A‴
E
B
B′
B″
B‴
E′
C
C′
C″
C‴
E″
D
D′
D″
D‴
E‴

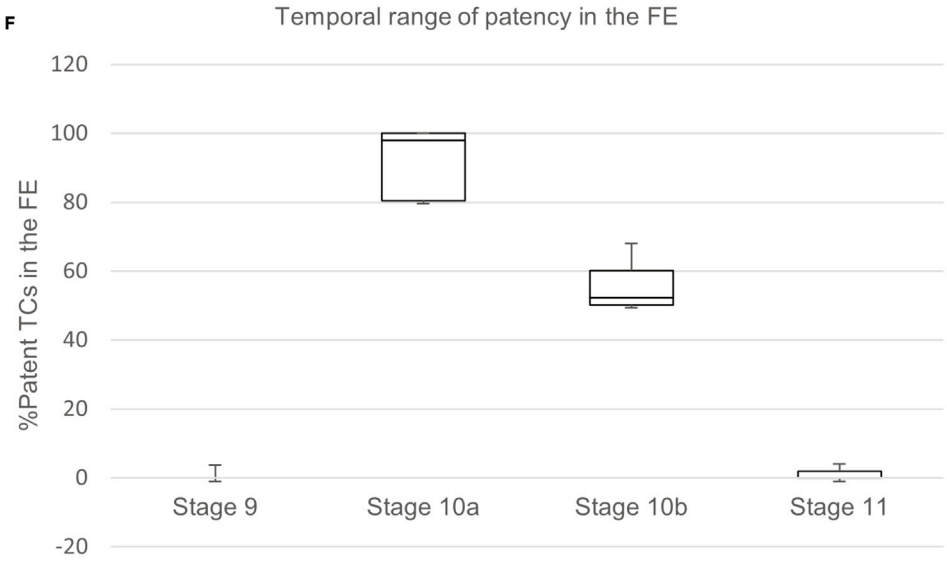
F
Temporal range of patency in the FE
%Patent TCs in the FE
120
100
80
60
40
20
0
-20
Stage 9
Stage 10a
Stage 10b
Stage 11

Figure 2. Temporal range of patency

(A–D) Projections of St9-St11 egg chambers; scale bars, 20 μm. Regions in the white box are expanded in (A′–A‴ to D′–D‴). Intact TCs at stages 9 and 11 (yellow arrowheads in [A″] and [D″], respectively) and patent TCs at stages 10a and 10b (red arrowheads in [B″] and [C″], respectively); scale bars, 2 μm.
(E–E‴) Illustrations of the FE at stages 9 through 11 depicting intact and patent TCs. Hts marks the membrane (green), and DAPI marks nuclei.
(F) Quantification of the incidence of patent TCs in the WT FE between stages 9 and 11 as percentage patent TCs per 50 gaps counted in 10 egg chambers at each stage (N = 500; data are represented as mean ± standard error of the mean [SEM]).

dextran was indeed present and accumulating in the TC gaps between the follicle cells at St 10a (Figures S1I–S1I‴), indicating that the "barrier" function of patent FE is compromised, potentially allowing for trans-epithelial transport.

Temporal range of patency

Unlike in other insects (e.g., *Rhodnius prolixus*) where patency is present in most vitellogenic stages (Huebner and Injeyan, 1980), we found that patent TCs in *Drosophila* FE are present only during mid-to-late vitellogenic stages (St 10a and 10b), suggesting a more limited temporal range (Figure 2A–2E‴). We quantified the incidence of patency in the FE between stages 9 and 11 by calculating the percentage of patent TCs (Figure 2F, n = 50), confirming the onset of patency at St 10a, and its termination at St 11.

Visualizing various epithelial markers using immunostaining revealed a dynamic pattern of junction and adhesion proteins in the TCs over the course of patency (Figures S2A–S2T′). Septate junctions, marked by discs large, appear to be lower at TCs during patent stages and are restored at stage 11 when the gaps disappear (Figures S2A–S2D′). Adherens junctions, represented by E-cadherin (E-cad), are not observed at the TCs in patent epithelia but are present at TCs when patency is terminated at St 11 (Figures S2E–S2H′). In contrast, cortical F-actin remains intact and continuous through mid-vitellogenesis, although marginally reduced, indicating that the membrane and its associated cortical actin remain continuous even in patent FE (Figures S2I–S2L′). The tricellular junction (TCJ) septate junction protein Gliotactin (Gli) (Genova and Fehon, 2003), however, only appears at the TCs starting at late stage 10b (Figurse S2M–S2P′), coincident with the cessation of patency. The accumulation of Gli at TCs suggests the assembly of the TCJs—at least the tricellular septate junctions—at the termination of patency. Additionally, the extracellular matrix protein laminin accumulates in the gaps at St 10b (Figures S2Q–S2T′), indicating the possibility of basement membrane components also being transported across the epithelium, perhaps to aid in the closing or maintenance of the TCs post-patency.

Next, to determine potential regulators of the temporal range of patency, we performed an RNAi screen for transcription factors, adhesion and junction proteins, and hormone response elements previously reported to be active during mid-oogenesis and identified Ttk69—a zinc finger transcription factor, as a potential regulator. Ttk69 coordinates FE morphogenesis by regulating expression levels and localization of adhesion proteins such as E-cad (French et al., 2003; Boyle and Berg, 2009). Ttk69, previously reported to be expressed starting at St 10a, is also expressed during pre-vitellogenic and early vitellogenic stages (Figures S3A–S3D′). Knocking down *ttk69* in the FE resulted in an increased temporal range of patency, with ectopic TC gaps ranging from stage 9 to 11 (Figures 2A–2D‴′). We quantified the incidence of patent TCs in the *ttk69-RNAi* expressing FE as the percentage of patent TCs and show the expansion of the temporal range of patency in these egg chambers when compared to the WT control (Figure 3E compared to Figure 2F). The *ttk69* knockdown FE that presented premature patency at St 9 had no E-cad at the TCs at this stage (Figures S3E–S3E″), similar to the E-cad localization pattern in the cells of normally patent FE at St 10a (Figures S3F–S3F″). These data, therefore, suggest that Ttk69 plays a role in restricting the temporal range of patency in the FE. Overexpressing or knocking down E-cad in the FE is not sufficient to affect the TC gaps in patent FE (data not shown), indicating that the localization of E-cad rather than expression levels could affect patency under Ttk69.

Spatial pattern of patency is influenced by the dorsal anterior signals of the FE

Patency in *D. melanogaster* also showed a spatial pattern in the FE—specifically, the dorsal-anterior region has intact TCs while the rest of the FE TCs are patent at St 10b (Figures 4A–4B‴, 4H, and 4H′). This is also evident as a lower incidence of gaps at St 10b in the quantification of the temporal range of patency (Figure 2F). To quantify the spatial pattern in the incidence of patent TCs in the FE, the cross section of the FE was divided into four quadrants (I–IV representing the dorsal anterior (DA), dorsal posterior (DP), ventral

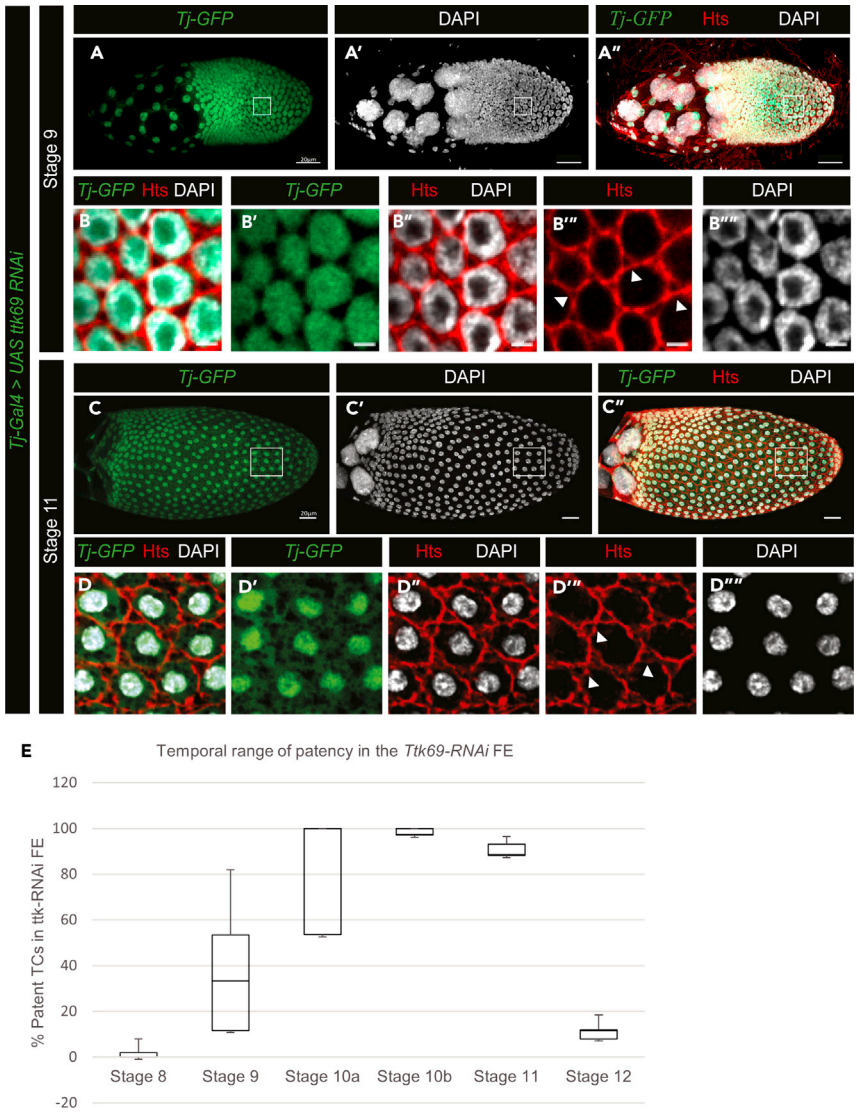

Figure 3. Ttk69 and the temporal range of patency

(A–D⁗) *UAS-ttk69-RNAi* expressing FE under *Tj-Gal4*, marked by *UAS-GFP*. *ttk69 KD* St 9 (A–A″) and St 11 (C–C″) egg chambers; scale bars, 20 μm; white boxes are enlarged in (B–B⁗) and (D–D⁗), respectively, both showing ectopic gaps (white arrowheads); scale bars, 2 μm. Hts marks the membrane (red), and DAPI marks nuclei.

(E) Quantification of the incidence of patent TCs in *Ttk69-RNAi* expressing FE between stages 8 and 12 as percentage patent TCs per 50 gaps counted in 5 egg chambers at each stage (N = 250; data are represented as mean ± SEM).

anterior (VA), and ventral posterior (VP), respectively) (Figure 4C). The percentage of patent TCs per (~10) TCs counted in 5 egg chambers verified the spatial pattern of patency (Figure 4C′).

The *Drosophila* FE is patterned along the anteroposterior and dorsoventral axes by the bone morphogenetic protein or decapentaplegic (Dpp) and epidermal growth factor receptor (EGFR) pathways, creating a subset of cells in the dorsal anterior with elevated levels of adhesion proteins (eg., E-cad, Fasciclin 3 [Fas3]) required for the formation of the respiratory tubes of the egg, called the dorsal appendages later in oogenesis (Neumann-Silberg and Schupbach, 1993; Twombly et al., 1996; Berg, 2005) (Figures S4A–S4B⁗). Ectopic expression of Dpp in the whole FE using the *CY2-Gal4* driver (Figures S4C–S4E′) resulted in elevated E-cad and Fas3 levels across the FE (Figures S4F–S4G″), and all TCs remained intact at St 10a (Figures 4D–4E″, illustrated in 4I and 4I′). In contrast, removal of EGFR (Epidermal Growth Factor Receptor) signaling by expressing a dominant negative form of EGFR in the FE resulted in the loss of E-cad and Fas3

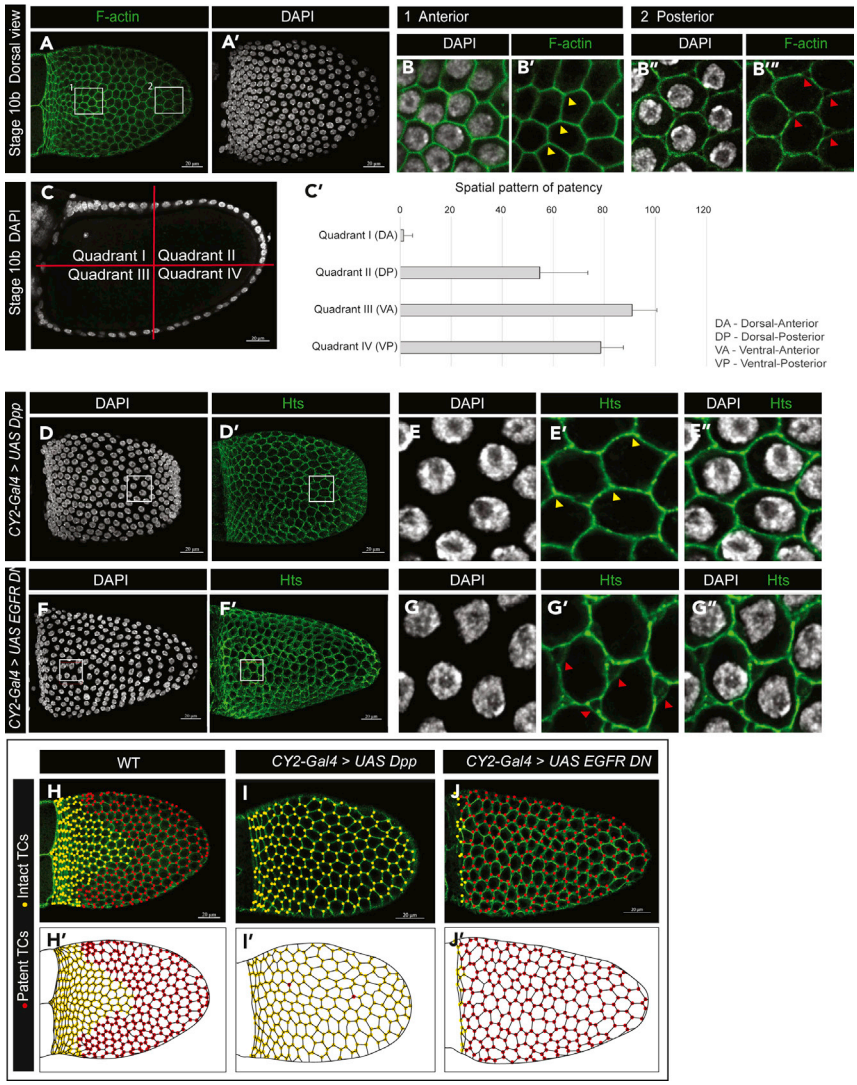

Figure 4. Spatial pattern of follicular patency and regulation

(A–B‴) (A–A″) Dorsal view of a St 10b egg chamber. Box#1 in the dorsal anterior is enlarged in (B–B′) showing intact TCs (yellow arrowheads); box#2 in the dorsal posterior is enlarged in (B″–B‴) showing patent TCs (red arrowheads).
(C–C′) Quantification of patent TCs in stage 10b egg chambers. (C) Cross section of a St 10b egg chamber depicting division into quadrants for quantification of percentage patent TCs per TCs counted. (C′) Spatial pattern of patency quantified as the average percentage patent TCs in the quadrants I-IV representing DA, DP, VA, and VP, respectively (10 TCs counted per quadrant in 15 egg chambers; N = 150; data are represented as mean ± SEM).
(D–J′) (D–D′) Dorsal view of a *UAS-Dpp* expressing FE. White box is enlarged in (E–E″) showing absence of patency (yellow arrowheads). (F–F′) Dorsal view of *UAS-EGFR-DN* expressing FE. White box is enlarged in (G–G″) showing ectopic patency in the dorsal anterior (directly above the oocyte nucleus) (red arrowheads). (H–J′) Illustration of the spatial pattern of patency, with yellow dots marking intact TCs and red dots marking patent TCs in WT (H–H′), *UAS-Dpp* (I–I′), and *UAS-EGFR-DN* (J–J′) expressing FE. Scale bars, 20 μm.

(Figures S4H–S4I″) and ectopic patency in the dorsal anterior FE, thus eliminating the spatial pattern of patency (Figures 4F–4G″, illustrated in 4J and 4J′). Together, our data therefore indicate that the spatial distribution of patency reported here is influenced by the dorsal-anterior Dpp and EGFR signaling pathways.

Patency for oocyte lipid uptake and growth

During oogenesis, lipid levels show a marked increase in the oocyte at St 10a (Sieber and Spradling, 2015), which, incidentally, is also when we have found the TC gaps to appear in the FE. Indeed, our TEM pictures

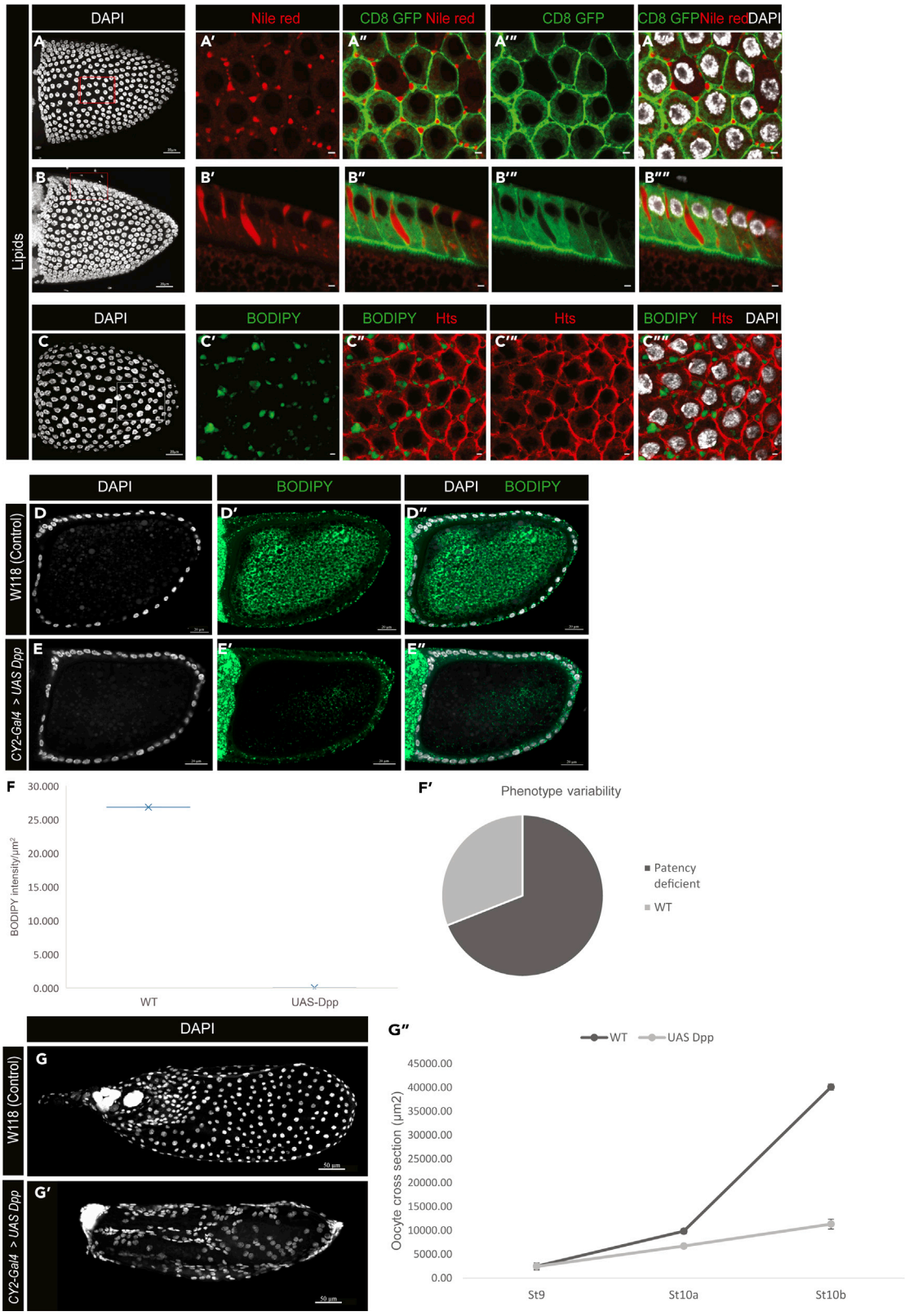
DAPI
Nile red
CD8 GFP Nile red
CD8 GFP
CD8 GFPNile redDAPI
Lipids
A
A′
A″
A‴
A⁗
B
B′
B″
B‴
B⁗
DAPI
BODIPY
BODIPY Hts
Hts
BODIPY Hts DAPI
C
C′
C″
C‴
C⁗
DAPI
BODIPY
DAPI BODIPY
W118 (Control)
CY2-Gal4 > UAS Dpp
D
D′
D″
E
E′
E″
F
BODIPY intensity/µm²
30.000
25.000
20.000
15.000
10.000
5.000
0.000
WT
UAS-Dpp
F′
Phenotype variability
Patency deficient
WT
DAPI
W118 (Control)
CY2-Gal4 > UAS Dpp
G
G′
50 µm
G″
WT
UAS Dpp
Oocyte cross section (µm2)
45000.00
40000.00
35000.00
30000.00
25000.00
20000.00
15000.00
10000.00
5000.00
0.00
St9
St10a
St10b

Figure 5. Patency for lipid uptake by the oocyte at St 10a

(A–C‴) Lipids are present in the gaps in patent FE. (A–B‴) Nile red staining shows lipids in the TC gaps and spanning the FE. Basal and cross-sectional views (A′–A‴ and B′–B‴, respectively). CD8-GFP marks the membrane. (C–C‴) BODIPY493/503 (green) confirms presence of lipids in the gaps. Membrane is marked by Hts (red).

BODIPY staining of control WT St 10a egg chamber (D–D″) and *UAS-Dpp* expressing FE lacking patency showing reduced levels of oocyte lipids at St 10a (E–E″). Note FE lipid globules are present in both.

(F) Quantification of the intensity of BODIPY signal per unit area in oocytes surrounded by *UAS-Dpp* expressing FE and WT FE at St 10a (N = 10).

(F′) Phenotype variation observed indicating FE lacking TC gaps and FE with WT phenotype (TC gaps present).

(G and G′) Later stage egg chambers with WT FE and *UAS-Dpp* expressing FE, resulting in abnormal egg chambers.

(G″) Quantification of cross-sectional area of the oocyte as a measure of oocyte growth in WT egg chambers and patency-lacking egg chambers with *UAS-Dpp* expressing FE (N = 10; data are represented as mean ± SEM). DAPI marks the nuclei. Scale bars: (A-C) and (E-F″), 20 μm; (A′-C‴), 2 μm; (G-G′), 50 μm.

showed material that could possibly be lipids in the gaps of patent FE (Figure S1C, yellow arrowheads). Further investigation using neutral lipid dyes Nile red and BODIPY revealed that lipids were present in the TC gaps and appeared to accumulate in these TC gaps (Figures 5A–5C‴). We therefore hypothesized that the TC gaps present in patent FE could facilitate the passage of lipids across the epithelial monolayer to be subsequently sequestered into the oocyte. To test this model, we used egg chambers lacking FE patency generated by expressing *UAS-Dpp* in the FE to check oocyte lipid levels in the absence of TC gaps. The *CY2-Gal4* driver ensures that the *UAS-Dpp* transgene expression is restricted only to the oocyte-associated follicle cells beginning at stage 10a Figures S4C–S5E′). Thus, the oocyte itself is unaffected by this experimental manipulation. This system effectively allowed us to isolate the direct effects of the expansion of the Dpp domain, one of which is the absence of TC gaps (Figures 4D–4E″, phenotype variance in St 10b egg chambers shown in Figure 5F′). BODIPY staining of these egg chambers with FE lacking patency showed a reduction in the oocyte lipid levels at stage 10a (Figures 5D–5E″, quantified in (F); N = 10). Additionally, the lipid uptake by the follicle cells in the *UAS-Dpp* expressing FE is comparable to that of WT FE, as indicated by the presence of BODIPY-stained lipid globules in both backgrounds (Figures 5D–5E″), indicating that the process of follicle cell lipid uptake is not affected by the ectopic *Dpp* overexpression.

During normal oogenesis, between St 10a and 11, the oocyte undergoes a dramatic increase in size (Kolahi et al., 2009). The egg chambers that do not have patent FE do not exhibit this exponential oocyte growth (Figure 5G″) and develop into abnormal late-stage follicles, in addition to the expected lack of dorsal appendages as a consequence of ectopic *UAS-Dpp* expression (Figures 5G and 5G′). These findings support the hypothesis that the inter-follicular gaps created during patent stages could play a role in the transepithelial transport of lipids across the FE for uptake by the oocyte.

Endosymbionts such as *Spiroplasma pulsonii* enter the oocyte from the maternal hemolymph in mid-vitellogenesis (Herren et al., 2013), and we asked whether patency assists in this vertical transfer. Staining egg chambers for the endosymbiont *S. pulsonii*, we found that some of these bacteria are observed between the follicle cells prior to the onset of patency, while heavily populating the TC gaps at St 10a and 10b (Herren et al., 2013) (Figures S5A–S5B″). In FE lacking patency, *S. poulsonii* was still detected between the follicle cells as in earlier stages of vitellogenesis (Figures S5C–S5D″). These data suggest that although the endosymbionts populate the TC gaps in patent FE, they could still move across the epithelium between the cells, similar to early stages.

D. simulans FE presents similar spatiotemporal patterns of patency

To determine whether the temporal range and spatial pattern of patency are unique to *D. melanogaster*, we examined the meroistic ovaries of the sister species *D. simulans*. The FE of only St 10a and St 10b egg chambers has patent TCs in *D. simulans* as well (Figures 6A–6D‴). The oocyte-associated FE of St 10b egg chambers in *D. simulans* also presented a similar spatial pattern of patency as in *D. melanogaster*, with intact TCs in the dorsal anterior region (Figures 6E–6F″). Together, our data indicate that the temporal and spatial patterns of patency are consistent in these sister species.

DISCUSSION

In this study, we report that *Drosophila melanogaster* exhibits a phase in oogenesis when the oocyte-associated FE develops "gaps" at TCs that extend across the monolayer, creating channels in the epithelium, a

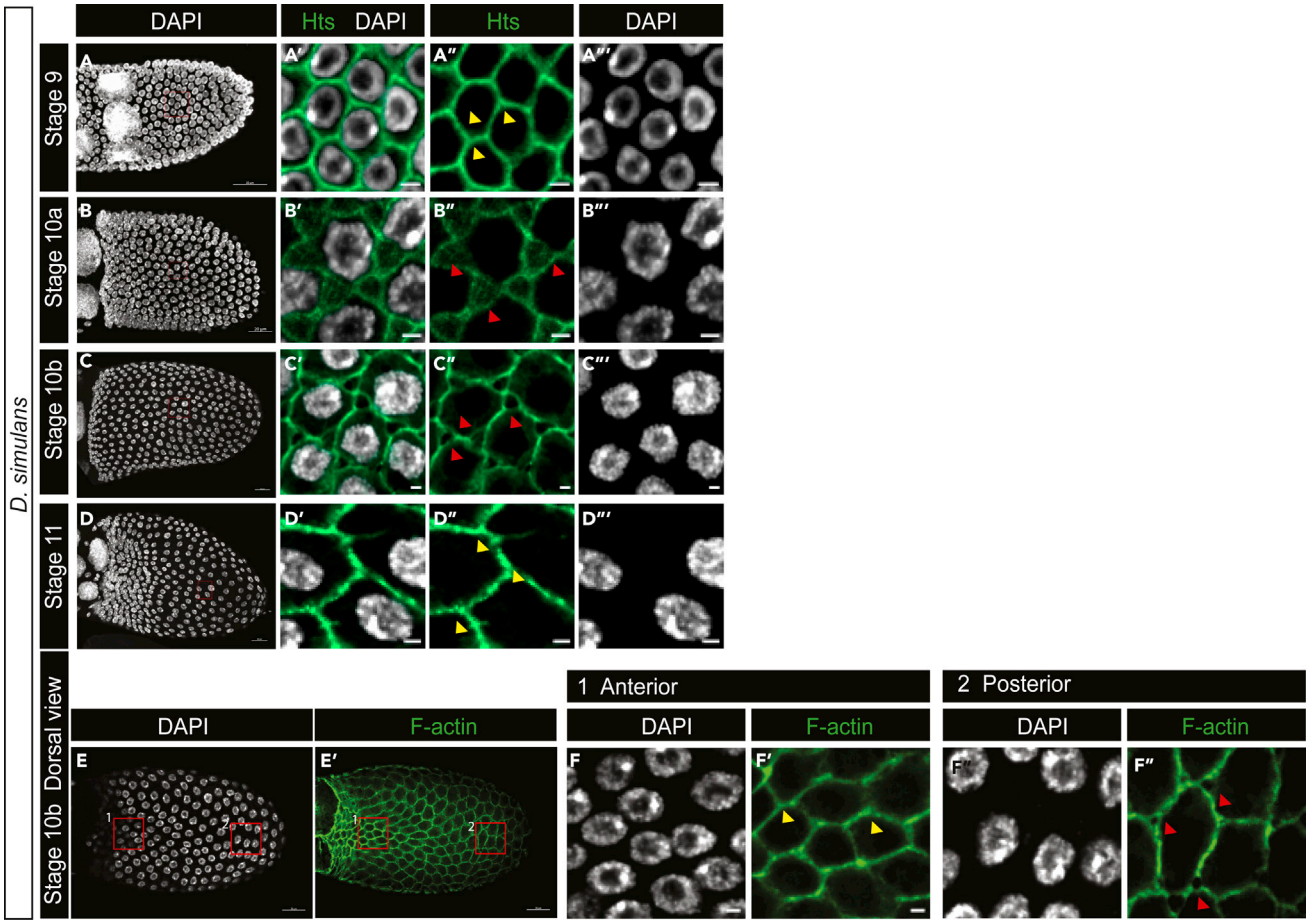

Figure 6. Temporal range and spatial pattern are conserved in *Drosophila simulans*

(A–D‴) Temporal range of patency in *D. simulans*. St 10a (B-B‴) and St 10b (C-C‴) show TC gaps characteristic of patency, while St 9 (A-A‴) and St 11 (D-D‴) have intact TCs.

(E–F″) Spatial pattern of patency in *D. simulans* is similar to that in *D. melanogaster*. (E–E″) Dorsal view of a stage 10b egg chamber in *D. simulans*. Box 1 in the dorsal anterior is expanded in (F and F′) showing intact TCs (yellow arrowheads). Box 2 in the dorsal posterior is expanded in (F″ and F‴) showing TC gaps (red arrowheads). Scale bars: (A–D) and (E-E′), 20 μm; (A′–D″) and (F–F″) 2 μm.

process previously referred to as "patency" in other insects (Telfer, 1961; Pratt and Davey, 1972; Zimowska et al., 1994). The FE, whose primary function over oogenesis is to assist in the development of the underlying oocyte and maintain an intact epithelial barrier around the egg chamber, appears to be perforated with TC gaps. Here, we illustrate spatiotemporal regulation of patency by the axial patterning signals of the FE (Dpp and EGFR) and potentially at a transcriptional level by Ttk69. Based on our findings in the *D. melanogaster* system, we now propose a conceptual model for patency involving the transient opening of TCs in the FE during mid-oogenesis, with a spatial pattern that is influenced by the patterning pathways of the FE and could assist in the transepithelial transport of lipids across the FE for oocyte growth (Figure 7).

Studies on patency in multiple insect species have reported that TC gaps are present across all vitellogenic stages of oogenesis (Telfer, 1961; Pratt and Davey, 1972; Zimowska et al., 1994; Abu-Hakima and Davey, 1977; Bai and Palli, 2016; Davey et al., 1993). In *Drosophila*, however, we discovered a more limited temporal range of patency. One of the key differences is the use of the meroistic *Drosophila* ovary (each egg chamber has an oocyte and nurse cells, all enclosed in the FE monolayer) in our study, while the models previously used are all species with panoistic ovaries (egg chambers consist of one oocyte surrounded by an epithelial monolayer of follicle cells, and no nurse cells) (King and Koch, 1963; Klowden, 2013), such as *Rhodnius proxilus*, *Locusta migratoria*, and *Tribolium castaneum* (Abu-Hakima and Davey, 1977; Bai and Palli, 2016; Davey et al., 1993). The nurse cells in meroistic ovaries function to synthesize and deposit essential nutrients, proteins, and RNA into the developing oocyte (King and Koch, 1963). We

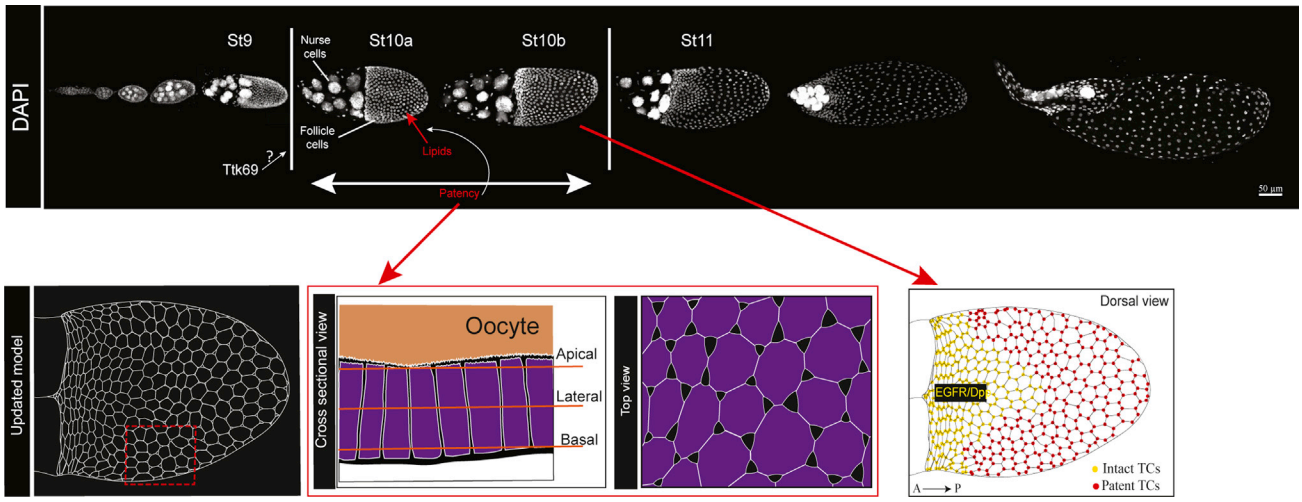

Figure 7. Model of follicular patency regulation in *Drosophila melanogaster*

DAPI stained egg chambers as arranged in an ovariole, depicting germarium to St 13. Patency is observed in the oocyte-associated follicular epithelium as gaps between the cells from the basal to the apical domain, illustrated in the cross-sectional and top-down views. The strict temporal range of patency (St10a–10b) is regulated by Ttk69, and the mechanistic details are yet to be discovered. At stage 10b, the dorsalizing signals EGFR and Dpp create a spatial pattern of patency, illustrated as "intact TCs" at the dorsal anterior and "patent TCs" in the rest of the FE.

therefore speculate that the absence of nurse cells in panoistic ovaries could explain the longer temporal range of patency in these egg chambers, acting to allow the transepithelial transport of essential materials directly from the hemolymph over longer periods of time to compensate. Indeed, we confirmed the presence of TC gaps in all vitellogenic stages of the panoistic *B. germanica* ovaries (data not shown). Additionally, we observed a limited temporal range of patency in meroistic ovaries of other species of the Drosophilidae family as well, including *D. simulans* (Figure 6), *Zaprionus indianus*, and *Scaptodrosophila latifascieformis* (data not shown), further supporting this hypothesis.

The use of *CY2-Gal4* to drive the expression of genes vital for vitellogenic progression allowed us to isolate patent-stage specific effects of the regulators on the FE. The temporal range of patency correlates well with the dramatic increase in oocyte volume between St 10a and 10b (Kolahi et al., 2009), raising the possibility that patency could support the uptake of lipids and yolk by the oocyte, thereby contributing to the normal growth of the oocyte. This is, in part, supported by the lower levels of oocyte lipids and the apparent reduction of oocyte size observed in the egg chambers with *UAS-Dpp* expressing FE that lack the TC gaps (Figures 5D–5G″). This reduction in the oocyte growth could be attributed to the absence of gaps in the FE, or more broadly, to the change in cell identity under ectopic *Dpp* expression, one effect of which is the absence of patency. Future studies will have to address whether patency is indeed required for this transepithelial transport of lipids and perhaps yolk proteins across the FE.

The patterning of the FE by the Dpp and EGFR pathways is required for dorsal appendage formation during later oogenesis, when a pair of respiratory tubes is formed from the dorsal anterior cells of the epithelial monolayer. These cells present higher expression levels of a range of adhesion proteins such as Ecad and Fas3 (Neumann-Silberg and Schupbach, 1993; Twombly et al., 1996; Berg, 2005) (Figures S4A–S4B‴), which could lead to the absence of TC "gaps" in the FE in this region, thus generating the spatial pattern of patency we report in this study. Although ectopic expression of either Ecad or Fas3 was not sufficient to alter the formation of TC gaps, it is possible that a combination of these and other adhesion proteins together result in the intact TCs in the dorsal anterior FE. Another possibility is that the lack of patency in the dorsal anterior FE could have a functional significance. At St 10a of oogenesis, the columnar oocyte-associated follicular epithelium is formed, following multiple rearrangement and migration events (King and Koch, 1963), and as the egg chamber progresses through oogenesis from St 10b to 11, all the cells of the FE flatten, except those from the dorsal appendages—the same cells that do not exhibit patency. We can therefore speculate that the lack of patency at the dorsal anterior could "protect" the cells from flattening and hence assist in the formation of the dorsal appendages. Detailed genetic and biochemical studies would indeed reveal the significance of the spatial pattern of patency.

The spatial pattern of patency that we report here also generates a corresponding spatial pattern in the localization of lipids (Nile red) at the TCs, while the remaining FE presenting patent TCs has lipids in their TC gaps (Figure S6). Moreover, previous reports on vertical transfer of the endosymbiont *S. pulsonii* also report a posterior preference in the localization of the bacteria on the FE (Herren et al., 2013), indicating that the spatial pattern of patency could also influence the pattern of passage of these bacteria. Together, the spatial pattern of patency could indeed result in the spatial pattern of the transepithelial transport in the FE.

In several insects such as *R. proxilus*, *Locusta migratoria*, and *Tribolium castaneum*, the sesquiterpenoid juvenile hormone (JH) has been reported to be a major regulator of patency (Abu-Hakima and Davey, 1977; Bai and Palli, 2016; Davey et al., 1993). A complex interaction between the steroid hormone ecdysone and JH coordinates vitellogenic progression in *Drosophila* (Bownes, 1989; Postlethwait and Handler, 1979). Preliminary studies on the effects of ecdysone on the FE and patency (data not shown) indicate the possibility that patency in *Drosophila* could be affected by ecdysone as well as JH in *Drosophila*. Future experiments will aim to determine the role of these hormones in the regulation of patency.

The accumulation of Gli at TCJs only at the termination of patency in the *Drosophila* FE (Figures S2M–S2P′) suggests formation and/or reinforcement of the TCJs at the end of patency. Gli has been reported to be required at TCJs for epithelial barrier function (Genova and Fehon, 2003), and we found that the FE expressing *gli-RNAi* presented patent TCJs even at St11 (data not shown). Gli, although a central component of TCJ septate junctions (Genova and Fehon, 2003), is only one component of the TCJs in epithelia. Other known TCJ proteins and their regulators include Anakonda, the master regulator of Gli expression and localization (Byri et al., 2015), Sidekick, the TCJ adherens junction protein (Letizia et al., 2019; Finegan et al., 2019; Uechi and Kuranaga, 2020), and M6, the TCJ protein required for oogenesis (Zappia et al., 2011). It is possible that these and other TCJ proteins might be involved in the creation, maintenance, and termination of patency in the FE. An assessment of the chronological order of appearance, localization, and expression levels over the course of patency, in addition to functional studies, will help delineate the mechanistic details of patency in the FE.

A previous study of "open zones of contact (ZOCs)" reported the separation of apposed basolateral membranes in the *Drosophila* FE, and we propose that these open ZOCs are indeed the patent TCs we have characterized in detail here (Schotman et al., 2008). Our characterization of patency in this study and the mechanism of open ZOC closure together present a model of *Drosophila* FE behavior involving the transient opening of TCs for the non-typical epithelial process of patency.

Altogether, this study creates a platform for further research into epithelial behavior, TCJ assembly and dynamics, and transepithelial transport mechanisms across epithelial monolayers.

Limitations of study

While we provide consistent data suggesting the involvement of Ttk69 in the regulation of temporal range of patency, our experiments do not rule out off-target effects of RNAi. Further experiments to validate this phenotype will aim to validate the mechanistic role of Ttk69 in limiting the temporal range of patency in *Drosophila*. Additionally, our data supporting the hypothesis that patency is required for the transepithelial transport of lipids across the FE are indirect. Combined with live imaging and a more pointed approach, perhaps by modifying TCJ dynamics in the FE during patent stages to generate FE lacking patency, combined with the Dpp overexpression system used here, it would be possible to establish the functional aspects of patency in more detail and directly test the model we propose here.

Resource availability

Lead contact

Further information and requests for resources should be directed to and will be fulfilled by the lead contact, Wu-Min Deng (wdeng7@tulane.edu).

Materials availability

The study did not generate any unique reagents.

Data and code availability

This article includes all data sets generated or analyzed during this study.

METHODS

All methods can be found in the accompanying transparent methods supplemental file.

SUPPLEMENTAL INFORMATION

Supplemental information can be found online at https://doi.org/10.1016/j.isci.2021.102275.

ACKNOWLEDGMENTS

We thank Drs. V. Auld, C. Berg, D. Houle, B. Lemaitre, R. Xi, Developmental Studies Hybridoma Bank (DSHB, USA), and Bloomington Drosophila Stock Center (BDSC, USA) for antibodies and fly stocks. We acknowledge the assistance of the UT Southwestern Electron Microscopy Core Facility for acquiring TEM images. We thank members of the Deng Laboratory for valuable discussions and support, especially Hongcui Bao for assistance with live imaging and P. Michael Albert II for assistance with editing the manuscript. W.-M. D. was supported by NIH R01 GM072562, R01 CA224381, R01 CA227789 and NSF IOS-1552333.

AUTHOR CONTRIBUTIONS

Conceptualization, methodology, validation, investigation, visualization, and project administration, S.R. and W.-M.D.; writing – original draft, S.R.; writing – review & editing, S.R., Y.-C.H., and W.-M.D.; supervision and funding acquisition, W.-M.D.

DECLARATION OF INTERESTS

The authors declare no competing interests.

Received: March 10, 2020
Revised: February 19, 2021
Accepted: March 2, 2021
Published: April 23, 2021

REFERENCES

Abu-Hakima, R., and Davey, K.G. (1977). The action of juvenile hormone on the follicle cells of Rhodnius Prolixus: the importance of volume changes. J. Exp. Biol. *69*, 33–44.

Bai, H., and Palli, S.B. (2016). Identification of G protein-coupled receptors required for vitellogenin uptake into the oocytes of the red flour beetle, *Tribolium castaneum*. Sci. Rep. *6*, p27648.

Berg, C.A. (2005). The *Drosophila* shell game: patterning genes and morphological change. Trends Genet. *21*, 346–355.

Bosveld, F., Wang, Z., and Bellaïche, Y. (2008). Tricellular junctions: a hot corner of epithelial biology. Curr. Opin. Cell Biol. *54*, 80–88.

Bownes, M. (1989). The roles of juvenile hormone, ecdysone and the ovary in the control of *Drosophila* vitellogenesis. J. Insect Physiol. *35*, 409–413.

Bownes, M., Ronaldson, E., Mauchline, D., and Martinez, A. (1993). Regulation of vitellogenesis in *Drosophila*. Int. J. Insect Morphol. Embryol. *22*, 349–367.

Boyle, M.J., and Berg, C.A. (2009). Control in time and space: tramtrack69 cooperates with Notch and Ecdysone to repress ectopic fate and shape changes during *Drosophila* egg chamber maturation. Development *136*, 4187–4197.

Byri, S., Misra, T., Syed, Z.A., Bätz, T., Shah, J., Boril, L., Glashauser, J., Aegerter-Wilmsen, T., Matzat, T., Moussian, B., et al. (2015). The Triple-Repeat protein Anakonda controls epithelial tricellular junction formation in *Drosophila*. Dev. Cell *33*, 535–548.

Davey, K.G., Sevala, V.L., and Gordon, R.B. (1993). The action of juvenile hormone and antigonadotropin on the follicle cells of *Locusta migratoria*. Invest. Reprod. Dev. *24*, 39–45.

DiMario, P.J., and Mahowald, A.E. (1987). Female sterile (1) yolkless: a recessive female sterile mutation in *Drosophila melanogaster* with depressed numbers of coated pits and coated vesicles within the developing oocytes. J. Cell Biol. *105*, 199–206.

Dobens, L.L., and Raftery, L.A. (2000). Integration of epithelial patterning and morphogenesis in *Drosophila* ovarian follicle cells. Dev. Dyn. *218*, 80–93.

Dunn, S., Rush, L., Lu, J.-Y., and Xu, T. (2018). Mutations in the *Drosophila* tricellular junction protein M6 synergize with RasV12 to induce apical cell delamination and invasion. Proc. Natl. Acad. Sci. U S A *115*, 8358–8363.

Finegan, T.M.1., Hervieux, N., Nestor-Bergmann, A., Fletcher, A.G., Blanchard, G.B., and Sanson, B. (2019). The tricellular vertex-specific adhesion molecule Sidekick facilitates polarised cell intercalation during *Drosophila* axis extension. PLoS Biol. *17*, e3000522.

French, R.L., Cosand, K.A., and Berg, C.A. (2003). The *Drosophila* female sterile mutation twin peaks is a novel allele of tramtrack and reveals a requirement for Ttk69 in epithelial morphogenesis. Dev. Biol. *253*, 18–35.

Genova, J.L., and Fehon, R.G. (2003). Neuroglian, Gliotactin, and the Na+/K+ ATPase are essential for septate junction function in *Drosophila*. J. Cell Biol. *161*, 979–989.

Guillot, C., and Lecuit, T. (2013). Mechanics of epithelial tissue homeostasis and morphogenesis. Science *340*, 1185–1189.

Herren, J.K., Paredes, J.C., Schüpfer, F., and Lemaitre, B. (2013). Vertical transmission of a *Drosophila* endosymbiont via cooption of the yolk transport and internalization machinery. mBio *4*, e00532–12.

Huebner, E., and Injeyan, H.S. (1980). Patency of the follicular epithelium in *Rhodnius prolixus*: a re-examination of the hormone response and technique refinement. Can. J. Zool. *58*, 1617–1625.

Isaac, P.G., and Bownes, M. (1982). Ovarian and fat-body vitellogenin synthesis in *Drosophila melanogaster*. Eur. J. Biochem. *123*, 527–534.

Jang, C., Starz-Gaiano, M., and Montell, D.J. (2007). Modeling migration and metastasis in *Drosophila*. J. Mammary Gland Biol. Neoplasia *12*, 103–114.

King, R.C., and Koch, E.A. (1963). Studies on the ovarian follicle cells of *Drosophila*. Q. J. Microsc. Sci. *104*, 297–320.

Klowden, M.J. (2013). Reproductive systems. In Physiological Systems in Insects, Third Edition, M.J. Klowden, ed. (Academic Press.), pp. 197–254.

Kolahi, K.S., White, P.F., Shreter, D.M., Classen, A.K., Bilder, D., and Mofrad, M.R. (2009). Quantitative analysis of epithelial morphogenesis in *Drosophila* oogenesis: new insights based on morphometric analysis and mechanical modeling. Dev. Biol. *331*, 129–139.

Letizia, A., He, D., Astigarraga, S., Colombelli, J., Hatini, V., Llimargas, M., and Treisman, J.E. (2019). Sidekick is a key component of tricellular adherens junctions that acts to resolve cell rearrangements. Dev. Cell *50*, 313–326.

Maloy, K.J., and Powrie, F. (2011). Intestinal homeostasis and its breakdown in inflammatory bowel disease. Nature *474*, 298–306.

Neuman-Silberberg, F.S., and Schupbach, T. (1993). The *Drosophila* dorsoventral patterning gene Gurken produces a dorsally localized RNA and encodes a TGF alpha-like protein. Cell *75*, 165–174.

Postlethwait, J.H., and Handler, A.M. (1979). The roles of juvenile hormone and 20-hydroxy-ecdysone during vitellogenesis in isolated abdomens of *Drosophila melanogaster*. J. Insect Physiol. *25*, 455–460.

Powell, D.W. (1981). Barrier function of epithelia. Am. J. Physiol. *241*, G275–G288.

Pratt, G.E., and Davey, K.G. (1972). The corpus allatum and oogenesis in *Rhodnius prolixus* (Stål.) 1. Effects of Allatectomy. J. Exp. Biol. *56*, 201–214.

Richard, D.S., Gilbert, M., Crum, B., Hollinshead, D.M., Schelble, S., and Scheswohl, D. (2001). Yolk protein endocytosis by oocytes in *Drosophila melanogaster*: immunofluorescent localization of clathrin, adaptin and the yolk protein receptor. J. Insect Physiol. *47*, 715–723.

Schotman, H., Karhinen, L., and Rabouille, C. (2008). dGRASP-mediated noncanonical integrin secretion is required for *Drosophila* epithelial remodeling. Dev. Cell *14*, 171–182.

Sieber, M.H., and Spradling, A.C. (2015). Steroid signaling establishes a female metabolic state and regulates SREBP to control oocyte lipid accumulation. Curr. Biol. *25*, 993–1004.

Tai, K., Cockburn, K., and Greco, V. (2019). Flexibility sustains epithelial tissue homeostasis. Curr. Opin. Cell Biol. *60*, 84–91.

Telfer, W.H. (1961). The route of entry and localization of blood proteins in the oocytes of saturniid moths. J. Biophys. Biochem. Cytol. *9*, 747–759.

Tufail, M., and Takeda, M. (2009). Insect vitellogenin/lipophorin receptors: molecular structures, role in oogenesis, and regulatory mechanisms. J. Insect Physiol. *55*, 88–104.

Twombly, V., Blackman, R.K., Jin, H., Graff, J.M., Padgett, R.W., and Gelbart, W.M. (1996). The TGF-beta signaling pathway is essential for *Drosophila* oogenesis. Development *122*, 1555–1565.

Uechi, H., and Kuranaga, E. (2020). Inhibition of a negative feedback for persistent epithelial cell–cell junction contraction by p21-activated kinase 3. https://doi.org/10.1101/743237.

Weiner, A.J., Goralsky, T.J., and Mahowald, A.P. (1982). The follicle cells are a major site of vitellogenin synthesis in *Drosophila*. Dev. Biol. *89*, 225–236.

Zappia, M.P., Brocco, M.A., Billi, S.C., Frasch, A.C., and Ceriani, M.F. (2011). M6 membrane protein plays an essential role in *Drosophila* oogenesis. PLoS One *6*, e19715.

Zimowska, G., Shirk, P.D., Silhacek, D.L., and Shaaya, E. (1994). Yolk sphere formation is initiated in oocytes before development of patency in follicles of the moth, *Plodia interpunctella*. Roux Arch. Dev. Biol. *203*, 215–226.

iScience, Volume *24*

Supplemental information

Developmental regulation of oocyte lipid intake through `patent' follicular epithelium in *Drosophila melanogaster*

Sarayu Row, Yi-Chun Huang, and Wu-Min Deng

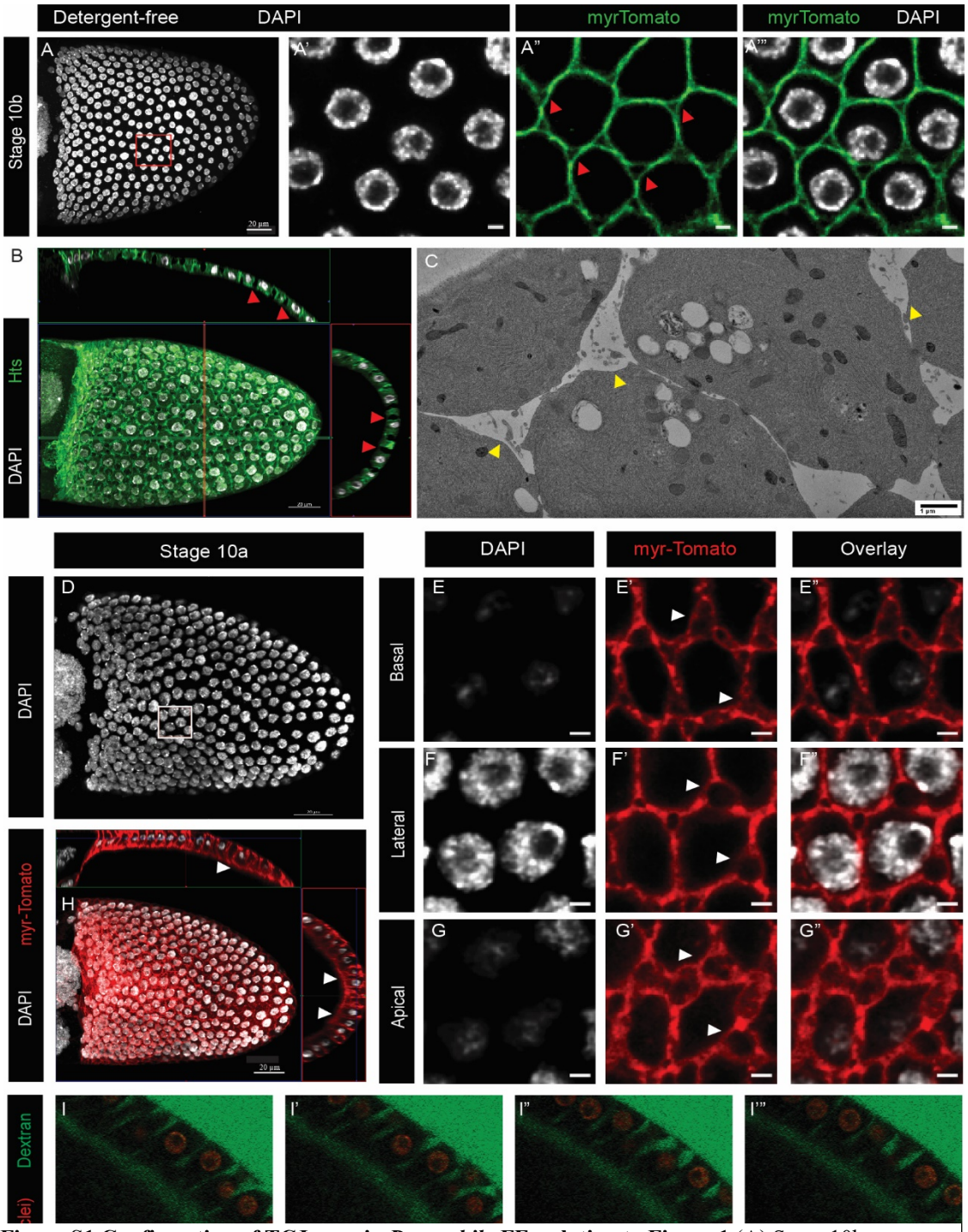

Figure S1 Confirmation of TCJ gaps in *Drosophila* FE, relating to Figure 1 (A) Stage 10b egg chamber expressing *Tj-Gal4, 10XUAS-myr-Td-Tomato*, fixed and mounted using a detergent-free protocol. Red box is enlarged in (A'-A"') showing patent TCs. (B) Ortho view of a projection of a St10a egg chamber with gaps across the FE (red arrowheads) Hts marks the membrane. (C) TEM image of a St10a egg chamber with material in the gaps (yellow arrowheads). (D-G") Stage 10a oocyte-associated FE expressing *10XUAS-myr-Td-Tomato*. White box is expanded in (E-G"). (E-E", F-F", G-G") Basal, lateral, and apical view, respectively. (H) Ortho view of a projection of a St10a *10XUAS-myr-Td-Tomato* expressing egg chamber, with gaps across the FE (white arrowheads). DAPI marks nuclei. (I-I"') Snapshots from live imaging of Stage 10a egg chamber expressing His2Av (marking nuclei), incubated in Dextran (green).

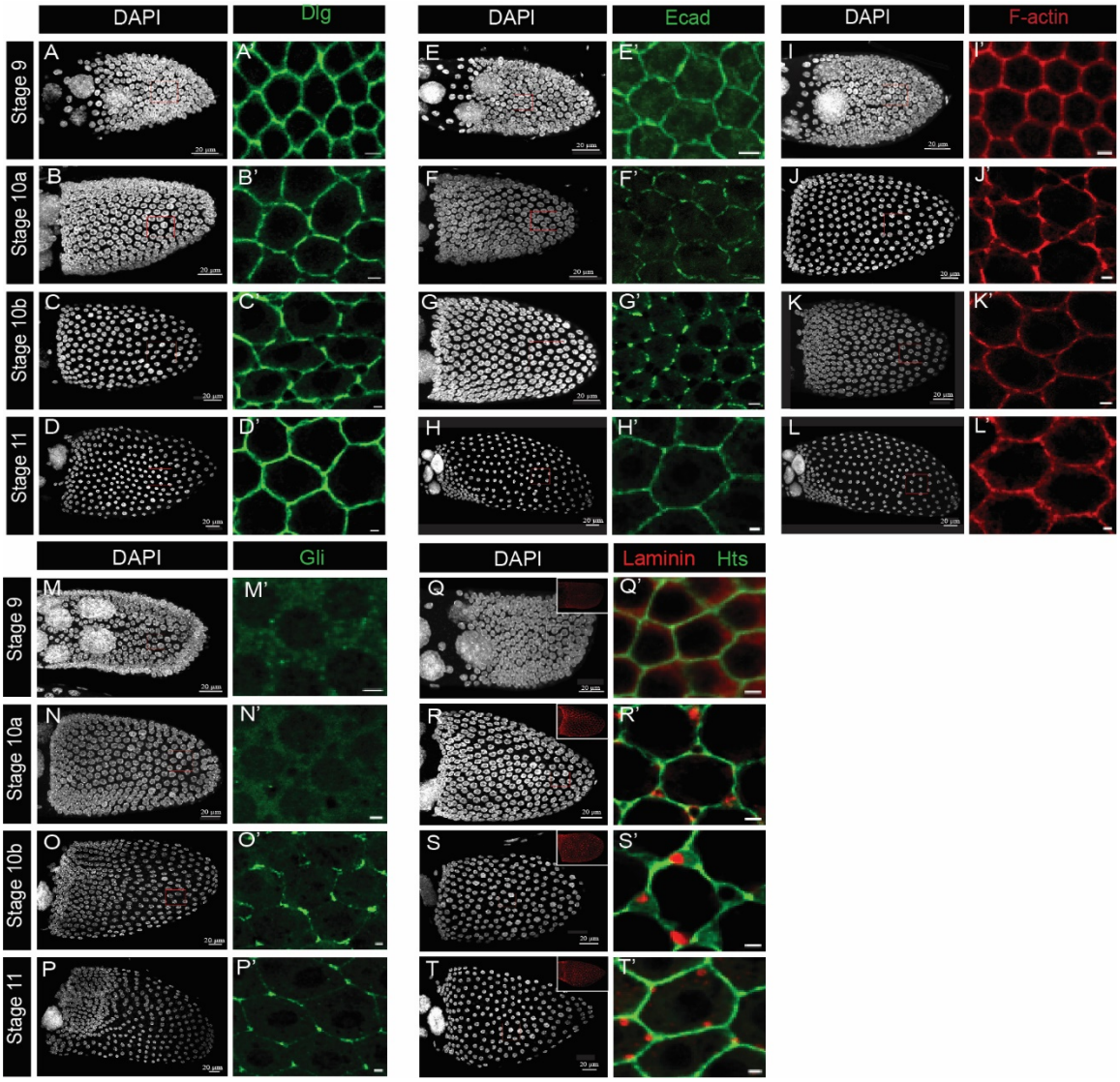

Figure S2 Characterization of adhesion and junction proteins over patency between stage 9 and 11, relating to Figure 2 Distribution of Septate junction protein Dlg (A-D'), adherens junction protein E-cadherin (E-H'), cortical F-actin (Phalloidin) (I-L'), tricellular septate junction protein, Gliotactin (Gli) (M-P'), and basement membrane component Laminin (Q-T'). Insets in (Q-T') Laminin in the full FE.

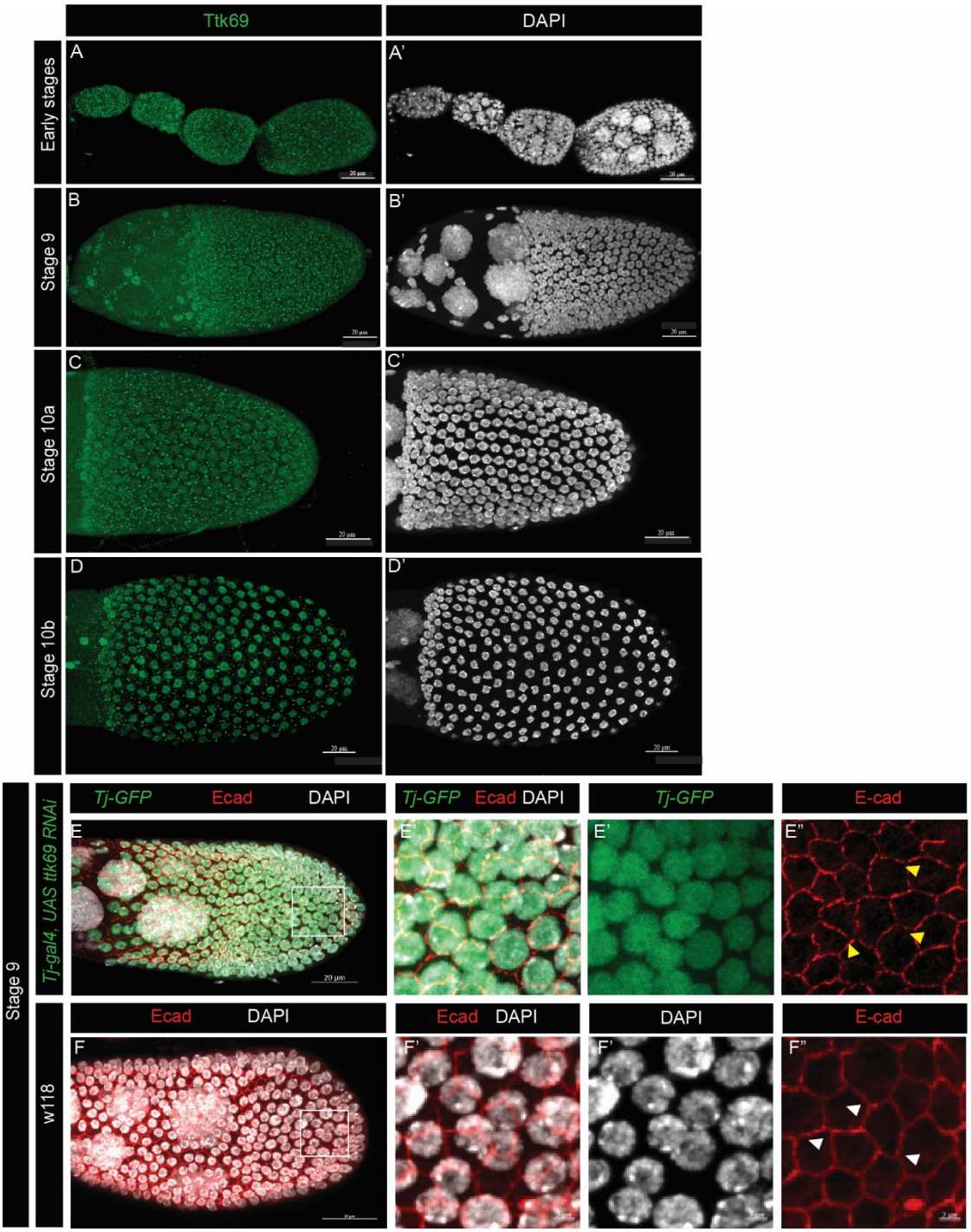

Figure S3 Ttk69 pattern in WT FE and *UAS-ttk-RNAi* expressing FE, related to Figure 3 (A-D') Egg chambers immunostained for Ttk69 protein. Punctate signals is background noise. (E-E") Stage 9 egg chamber expressing *UAS-ttk69-RNAi* under *Tj-Gal4*. White box is expanded in (E'-E"). E-cad is not present at TCs (yellow arrowheads). (F-F") Stage 9 wildtype egg chamber White box is expanded in (F'-F"). E-cad present at TCs (white arrowheads). DAPI marks the nucleus.

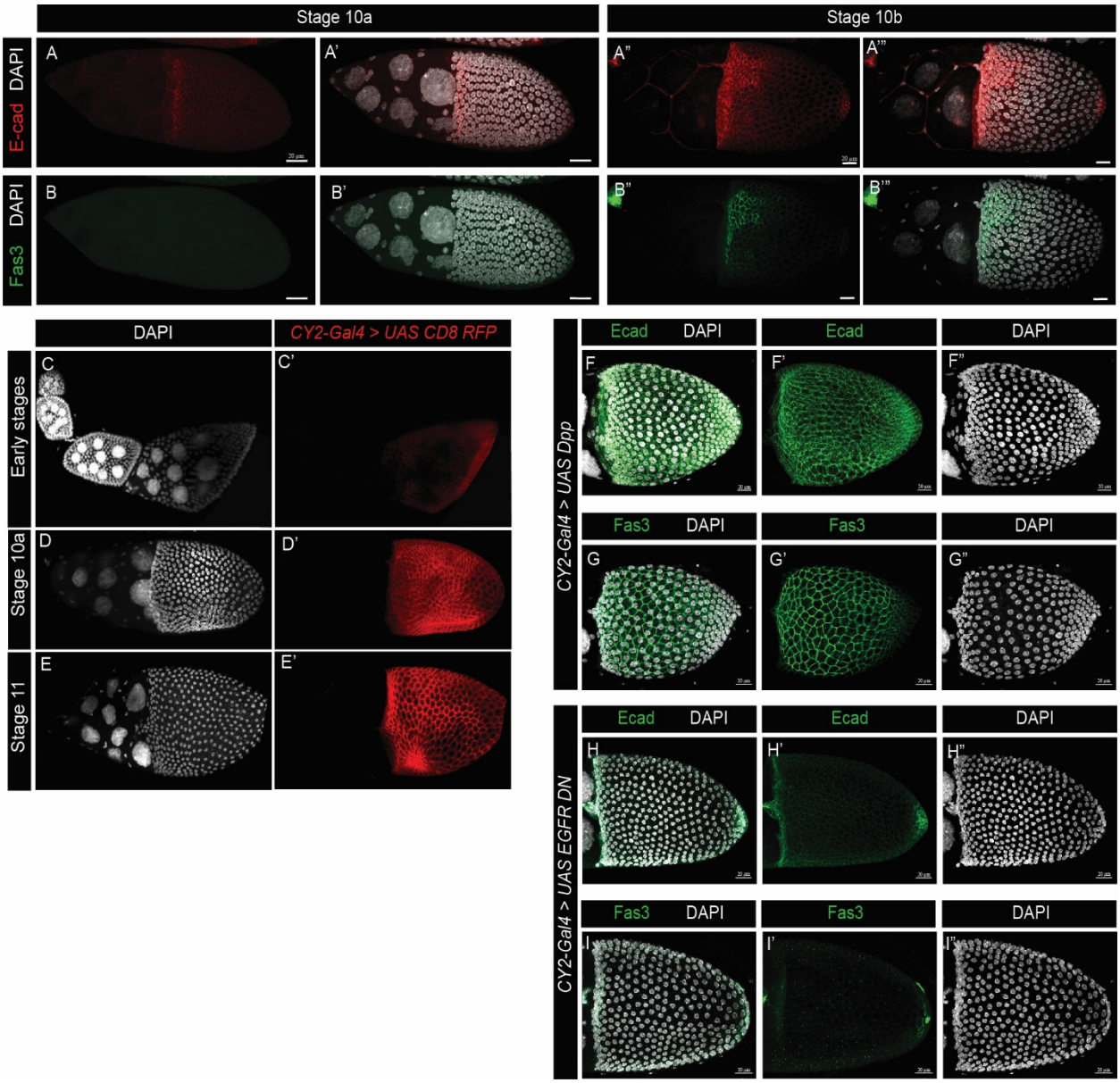

Figure S4 Dorsal pattern of adhesion proteins E-cad and Fas3, related to Figure 4 (A-B'") WT egg chambers with E-cad and Fas3 from St10a (A-A', B-B' respectively) to St10b (A"-A'", B"-B"', respectively). (C-E") *CY2-Gal4* expression pattern in *Drosophila* ovaries marked by *UAS-CD8:RFP* on the membrane. (F-G") Egg chambers expressing *UAS-Dpp* under *CY2-Gal4* driver. (H-I") Egg chambers expressing a dominant negative form of EGFR under UAS control using the *CY2-Gal4* driver.

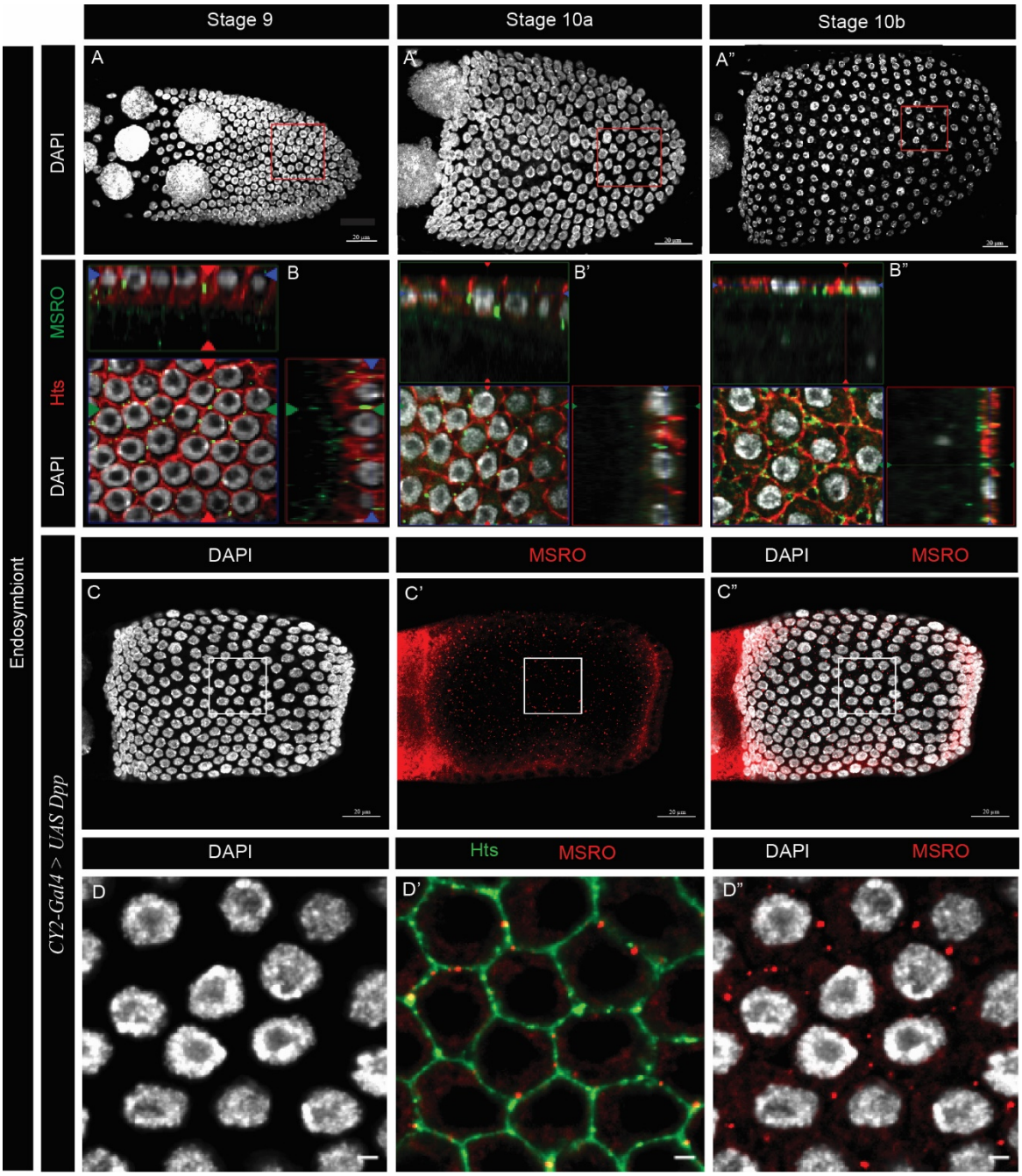

Figure S5 Vertical transfer of the endosymbiont *Spiroplasma pulsonii*, related to Figure 5 (A-A") Projections of DAPI stained Stage 9 – 11 egg chambers. Red boxed are enlarged in (B-B"), and ortho views are provided for top and cross-sectional views. (C-D") MSRO staining in *UAS-Dpp* expressing FE. MSRO marks the bacteria, Hts marks the membrane, and DAPI stains the nuclei.

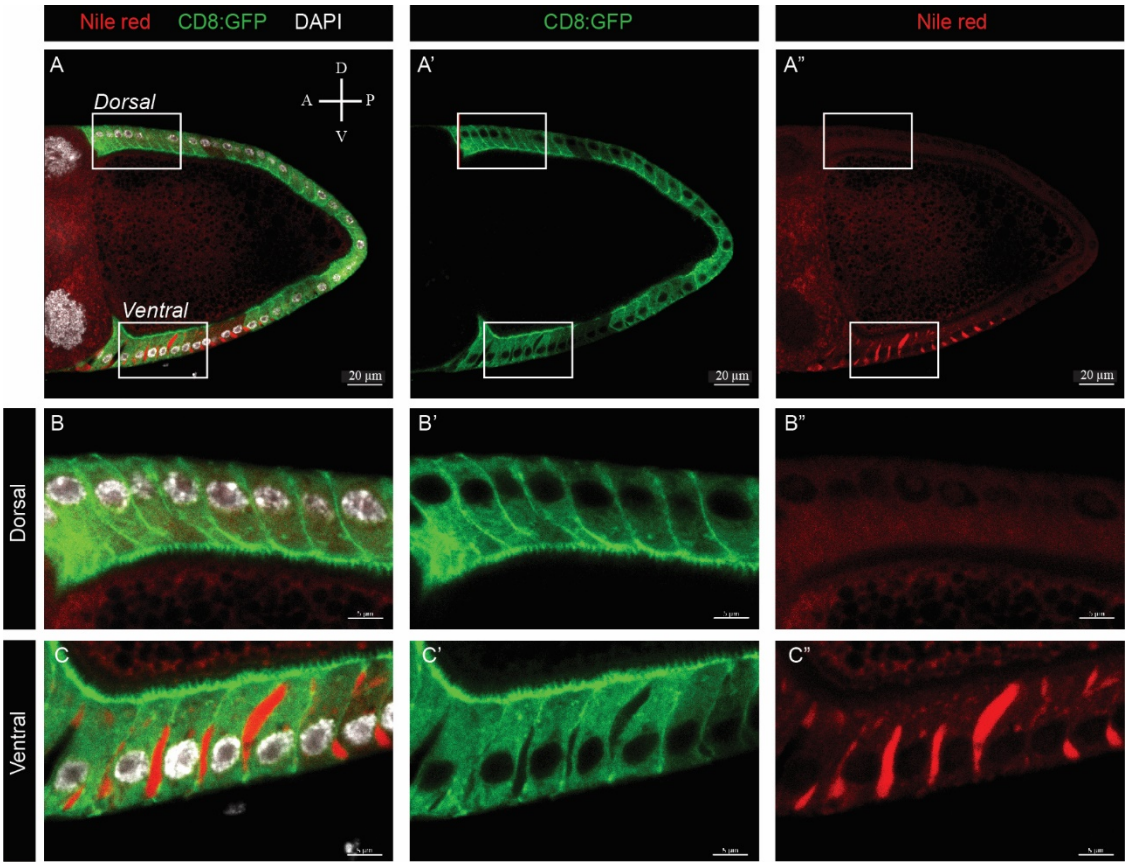

Figure S6. Spatial pattern of trans-epithelial transport of lipids across the FE, related to Figure 5. (A-A") Cross section of a *UAS-CD8:GFP* expressing egg chamber. White box labelled Dorsal is expanded in (B-B"); white box labelled Ventral is expanded in (C-C") showing TC gaps and lipids present between the cells in the patent TCs. Nile red marks lipids, DAPI marks nuclei.

Transparent methods

Drosophila strains and culture

All Drosophila stocks were maintained and crossed at 21–22°, unless otherwise indicated. The w[118] strain was used as the wild-type control. To control the temporal and regional gene expression targeting (TARGET) system, temperature-sensitive Gal80 (Gal80TS) under the ubiquitous tubulin driver was used to regulate the upstream activating sequence (UAS)-transgene expression by altering temperatures. Tj-Gal4 and CY2-Gal4 were used to drive UAS transgene expression in combination with Gal80TS. The crosses involving Gal80TS were crossed and maintained at 18˚C, and progeny were kept at 29˚C for 48hrs prior to dissection.

Tj-Gal4 is used to drive transgenes under UAS control in all the follicle cells across oogenesis. Transgenes that disrupt vitellogenic progression were used with CY2-Gal4, that drives transgenes under UAS control in only the oocyte associated follicle cells starting at low levels at St 9, and at high levels from St 10a [Fig. S4.(C-E')].

Fluorescence Microscopy and Image Analysis

Ovaries were dissected, fixed, and stained with antibodies using the protocol outlined below: (Adopted from Deng *et al*., 2001; Sun and Deng, 2005)
Ovaries were dissected in 1×PBS buffer and fixed for 10 minutes in 500µl of 4% paraformaldehyde. They were rinsed for 5 minutes with 1XPBT buffer and blocked in 20% goat serum (in PBT) for 2 hours at room temperature. The ovaries were then incubated in primary antibodies diluted in blocking buffer overnight at 4°C, followed by 4 10-minute PBT washes. They were then incubated in secondary antibodies for 2 hours at room temperature, and stained with DAPI (1µg/ml in PBT), washed three times with PBT (10 minutes each), and transferred onto slides in mounting solution (70% glycerol, 2%NPG, 1×PBS).

The following primary antibodies were used: Hu li tai shao (Hts) (1:5, 1B1), E-cadherin (Ecad) (1:20, DCAD2), Discs large (Dlg) (1:50, 4F3), and Fasciclin3 (Fas3) (1:15, 7G10) all from the Developmental Studies Hybridoma bank (DSHB), Laminin (gamma 1) (1:200, ab47651, Abcam), Gliotactin (1:50, a gift from Dr. Auld), MSRO (1:200, a gift from Dr. Lemaitre), Ttk69 (1:200, a gift from Dr. Xi). Alexa Fluor 488- or 546-conjugated goat anti-mouse and anti-rabbit secondary antibodies (1:400; Molecular Probes, Eugene, OR) were used. Phalloidin-546 (Invitrogen) was used to stain F-actin. Nuclei were labeled with DAPI (1:1000). Images were captured with Zeiss LSM 800 confocal microscope. Zeiss and ImageJ software were used for image analyses and processing.

Detergent-free protocol was modified from the standard protocol above, with all the same reagents prepared without Tween-20.

Lipid Staining

Ovaries were dissected in PBS and fixed in 4% PFA for 15 minutes. Following 2 washes with PBT, the ovaries were incubated in Nile red (TCI America, 7385-67-3) (0.002% dye diluted in PBT, adopted from 29) or BODIPY 493/503 (ThermoFisher Scientific, Cat No. D3922) (Stock: 1mg/ml BODIPY in absolute ethanol, Working: 1:500 in PBS) in dark for 30 minutes. Following 2 PBT washes, the ovaries were either stained with antibodies, or with DAPI, and then mounted onto slides.

Live imaging

Flies with RFP-tagged His2Av (BL 23650) were incubated in 25˚C with yeast paste for 2 days. Ovaries were dissected in the Schneider Drosophila Medium (Genesee Scientific, #25-512), then st9-st11 egg chambers were mounted in 1% low-melting agarose and cultured in freshly prepared imaging medium (Schneider Drosophila Medium with 15% fly extract, 0.5% penicillin/streptomycin, and 20μg/ml insulin) on cell imaging dishes (145 μm cover glass bottom, Eppendorf #30740009). Dextran-FITC (12.5ug/ml, Sigma # 46944) was added right before imaging started. Live images were taken using a Zeiss LSM 980 Confocal Microscope with Airyscan 2, and set 1hr duration. The imaging raw data were processed and prepared by the ZEN 3.0 software.

Transmission Electron Microscopy

The samples for TEM were prepared using the protocol outlined below: (adopted from Tamori et al., 2016, Matsumoto et al., 1988):
Tissue samples were fixed with Karnovsky's Fixative. After three rinses with 0.1 M sodium cacodylate buffer, samples were embedded in 3% agarose and sliced into small blocks (1mm3), rinsed with the same buffer three times and post-fixed with 1% osmium tetroxide and 0.8 % Potassium Ferricyanide in 0.1 M sodium cacodylate buffer for one and a half hours at room temperature. Samples were rinsed with water and en bloc stained with 4% uranyl acetate in 50% ethanol for two hours. They were then dehydrated with increasing concentration of ethanol, transitioned into propylene oxide, infiltrated with Embed-812 resin and polymerized in a 60°C oven overnight. Blocks were sectioned with a diamond knife (Diatome) on a Leica Ultracut 7 ultramicrotome (Leica Microsystems) and collected onto copper grids, post stained with 2% aqueous Uranyl acetate and lead citrate. Images were acquired on a JEM-1400 Plus transmission electron microscope equipped with a LaB6 source operated at 120 kV using an AMT-BioSprint 16M CCD camera.

Quantification and Statistical Analysis

All quantification data was analyzed by two-tailed Student's T-test. P-values were calculated using GraphPad Prism 8. Graphs were prepared in Excel. Sample sizes and p-values where appropriate are described in the main text, figures, or figure legends.

Supplementary references

Auld, V. J., Fetter, R. D., Broadie, K. & Goodman, C. S. (1995) Gliotactin, a novel transmembrane protein on peripheral glia, is required to form the blood-nerve barrier in *Drosophila*. *Cell*, **81(5)**, 757-767.

Deng, W.M., Althauser, C. & Ruohola-Baker, H. (2001) Notch-Delta signaling induces a transition from mitotic cell cycle to endocycle in *Drosophila* follicle cells. *Dev*., **128(23)**, 4737-4746.

Herren, J. K., Paredes, J. C., Schüpfer, F. & Lemaitre, B. (2013) Vertical Transmission of a *Drosophila* Endosymbiont Via Cooption of the Yolk Transport and Internalization Machinery. *mBio*., **4(2)**:e00532-12. doi: 10.1128/mBio.00532-12.

Matsumoto, E., Hirosawa, K., Takagawa, K. & Hotta, Y. (1988) Structure of retinular cells in a *Drosophila melanogaster* visual mutant, *rdgA*, at early stages of degeneration. *Cell Tissue Res*., **252**, 293–300.

Sun, J. J. & Deng, W-M. (2005) Notch-dependent downregulation of the homeodomain gene cut is required for the mitotic cycle/endocycle switch and cell differentiation in *Drosophila* follicle cells. *Dev*., **132**, 4299-4308.

Tamori, Y. T., Suzuki, E. & Deng, W-M. (2016) Epithelial tumors originate in tumor Hotspots, a tissue-intrinsic microenvironment. *PLoS Biol*., **14(9)**, e1002537. doi:10.1371/journal.pbio.1002537.

Wang, C., Guo, X., Dou, K., Chen, H., & Xi, R. (2015) Ttk69 acts as a master repressor of enteroendocrine cell specification in *Drosophila* intestinal stem cell lineages. *Dev*., **142**, 3321-3331.

Ward, E. J., Thaipisuttikul, I., Terayama, M., French, R. L., Jackson, S. M., Cosand, K. A., Tobler, K. J., Dorman, J. B. & Berg, C. A. (2002) Gal4 enhancer trap patterns during *Drosophila* development. *Genesis*, **34**, 46-50.